designed Dorfin-CHIP chimeric proteins containing both the hydrophobic substrate-binding domain of Dorfin and the U-box domain of CHIP, which has strong E3 activity (Fig. 2C). We verified that all of the 12 candidate chimeric proteins were expressed in HEK293 cells (Fig. 2D).

Expression of Dorfin-CHIP chimeric proteins in cells

The half lives of all the Dorfin-CHIP chimeric proteins were more than 1 h. In some of these proteins, such as Dorfin-CHIP$^{D, G, J}$, and ^{L}, moderate amounts of protein still remained at 6 h after labeling, indicating that they were degraded much more slowly than was Dorfin^{WT} (Fig. 3). Repetitive experiments using Dorfin-CHIP^{L} yielded a significant difference between the amount of Dorfin^{WT} and Dorfin-CHIP^{L} at 1 h and 3 h (Table 1).

E3 activity of Dorfin-CHIP chimeric proteins against mutant SOD1

Immunoprecipitation analysis demonstrated that Dorfin and CHIP bound to mutant SOD1^{G85R} in equivalent amounts and that all of the Dorfin-CHIP chimeric proteins interacted with mutant SOD1^{G85R} *in vivo*. Dorfin-CHIP$^{A, D, E, F, J, K}$, and ^{L} bound to the same or greater amounts of SOD1^{G85R} than did Dorfin, whereas Dorfin-CHIP$^{B, C, G, H}$, and ^{I} did not (Fig. 4A, upper panel). None of the Dorfin-CHIP chimeric proteins bound to SOD1^{WT} *in vivo*

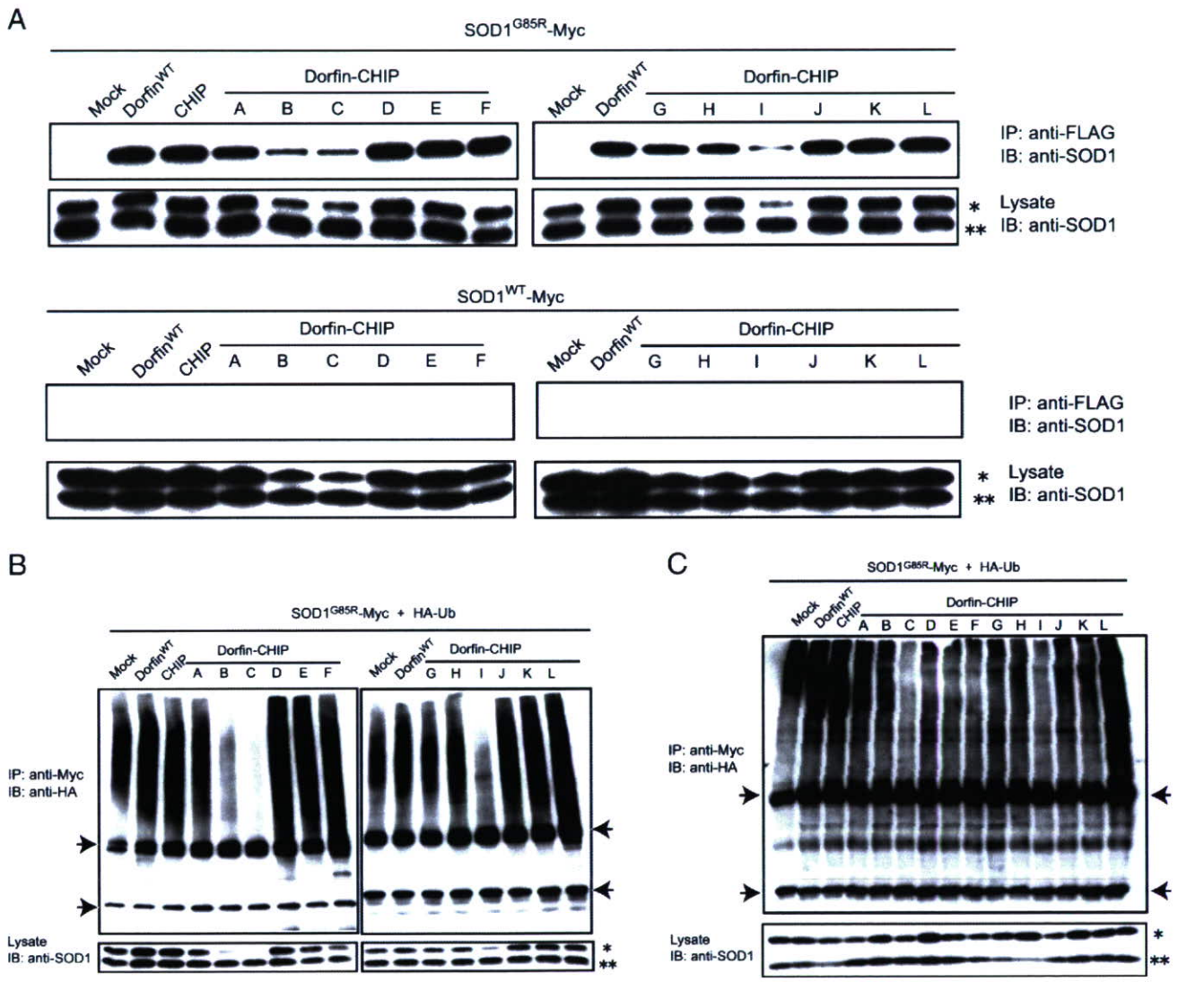

Fig. 4. The E3 activity of Dorfin-CHIP chimeric proteins on mutant SOD1 *in vivo*. (A) *In vivo* binding assay with both wild-type and mutant SOD1s. SOD1^{G85R}- or SOD1^{WT}-Myc and FLAG derivatives of Dorfin-CHIP chimeric proteins were coexpressed in HEK293 cells. Immunoprecipitation was done using anti-Myc antibody. Immunoblotting with anti-FLAG antibody revealed that all the Dorfin-CHIP chimeric proteins bound *in vivo* to SOD1^{G85R}-Myc but not to SOD1^{WT}-Myc. Single and double asterisks indicate overexpressed human SOD1s and mouse endogenous SOD1, respectively. (B) *In vivo* ubiquitylation assay in HEK293 cells. SOD1^{G85R}-Myc, HA-Ub, and FLAG derivatives of Dorfin-CHIP chimeric proteins were coexpressed in HEK293 cells. Immunoblotting with anti-HA antibody demonstrated the ubiquitylation level of SOD1^{G85R}-Myc by FLAG derivatives of Dorfin-CHIP chimeric proteins *in vivo*. Arrows indicate IgG light and heavy chains. Single and double asterisks indicate overexpressed SOD1 and mouse endogenous SOD1, respectively. (C) *In vivo* ubiquitylation assay in N2a cells. SOD1^{G85R}-Myc, HA-Ub, and FLAG derivatives of Dorfin-CHIP chimeric proteins were coexpressed in N2a cells. Arrows indicate IgG light and heavy chains. Single and double asterisks indicate overexpressed human SOD1s and mouse endogenous SOD1, respectively.

(Fig. 4A, lower panel). Some Dorfin-CHIP chimeric proteins, such as Dorfin-CHIP$^{B, C}$, and ^{I}, had lower amounts of both SOD1^{WT} and SOD1^{G85R} in the lysates. We performed quantitative RT-PCR using specific primers for SOD1-Myc, finding that coexpression of Dorfin-CHIP$^{B, C,}$ or ^{I} suppressed the mRNA expression of overexpressed SOD1 gene (Supplementary Fig. 1). Considering the possibility that these Dorfin-CHIP chimeric proteins might have unpredicted toxicity for cells by affecting gene transcription via unknown mechanisms, we excluded them from further analysis. Other Dorfin-CHIP proteins did not affect SOD1-Myc gene expression, which validated the comparison among IPs and ubiquitylated mutant SOD1 in Figs. 4A–C.

To assess the effectiveness of the E3 activity of Dorfin-CHIP chimeric proteins, we did an *in-vivo* ubiquitylation analysis by coexpression of SOD1^{G85R}-Myc, HA-Ub, and Dorfin-CHIP chimeric proteins in HEK293 cells. We found that Dorfin and CHIP enhanced the ubiquitylation of SOD1^{G85R} protein and that the ubiquitylation levels of these two E3 ligases were almost equivalent. Moreover, Dorfin-CHIP$^{D, E, F, J, K}$, and ^{L} ubiquitylated SOD1^{G85R} more effectively than did Dorfin or CHIP (Fig. 4B).

Performing the same *in-vivo* ubiquitylation assay using N2a cells, we observed that the levels of ubiquitylation of SOD1^{G85R} by Dorfin and CHIP were equivalent, as they were in HEK293 cells. Among Dorfin-CHIP chimeric proteins, only Dorfin-CHIP^{L}

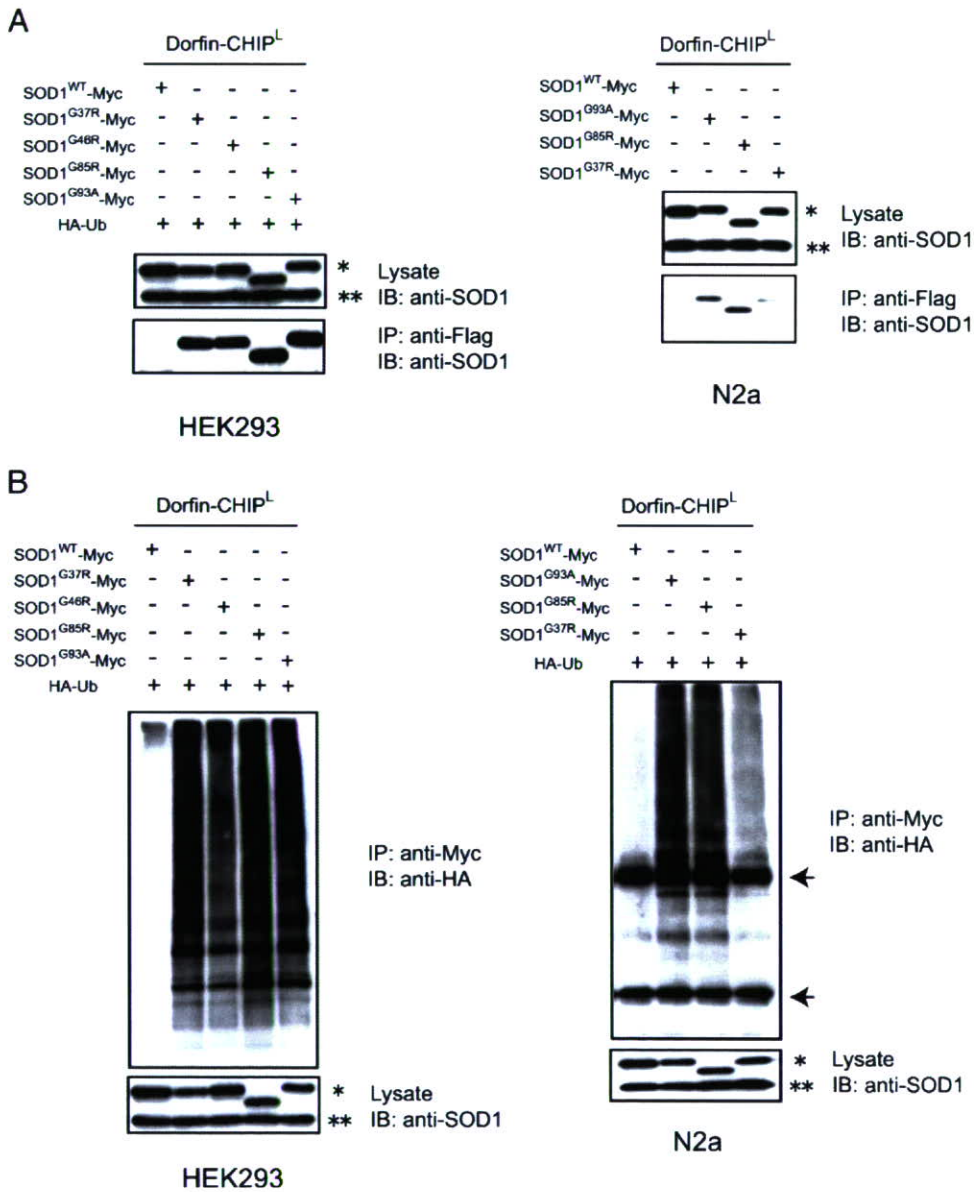

Fig. 5. Dorfin-CHIP^{L} specifically ubiquitylates mutant SOD1s *in vivo*. (A) *In vivo* binding assay with various mutant SOD1s. SOD1^{WT}-Myc, SOD1^{G93A}-Myc, SOD1^{G85R}-Myc, SOD1^{H46R}-Myc or SOD1^{G37R}-Myc, and FLAG-Dorfin-CHIP^{L} were coexpressed in HEK293 (left) and N2a cells (right). Immunoprecipitation was done using anti-Myc antibody. Immunoblotting with anti-FLAG antibody showed that both chimeric proteins specifically bound to mutant SOD1s *in vivo*. Single and double asterisks indicate overexpressed SOD1 and mouse endogenous SOD1, respectively. (B) *In vivo* ubiquitylation assay. SOD1^{WT}-Myc, SOD1^{G93A}-Myc, SOD1^{G85R}-Myc, SOD1^{H46R}-Myc or SOD1^{G37R}-Myc, as well as FLAG-Dorfin-CHIP^{L} and HA-Ub, was coexpressed in HEK293 (left) and N2a cells (right). Immunoblotting with anti-HA antibody showed the specific ubiquitylation of mutant SOD1-Myc by FLAG-Dorfin-CHIP^{L} *in vivo*. Arrows indicate IgG light and heavy chains. Single and double asterisks indicate overexpressed human SOD1s and mouse endogenous SOD1, respectively.

ubiquitylated SOD1^{G85R} more effectively than did Dorfin or CHIP, while Dorfin-CHIP$^{D, E, F, J}$, and ^{K} did not (Fig. 4C). Thus, Dorfin-CHIP^{L} was the most potent candidate of the chimeric proteins.

Ubiquitylation of mutant SOD1 by Dorfin-CHIP^{L}

Dorfin specifically ubiquitylated mutant SOD1 proteins, but not SOD1^{WT} protein (Niwa et al., 2002; Ishigaki et al., 2004). Similarly, Dorfin-CHIP^{L} interacted with SOD1^{G93A}, SOD1^{G85R}, SOD1^{H46R}, and SOD1^{G37R}, but not SOD1^{WT}, in HEK293 cells. This was confirmed in N2a cells (Fig. 5A). In both HEK293 and N2a cells, Dorfin-CHIP^{L} also ubiquitylated mutant SOD1 proteins but not SOD1^{WT} (Fig. 5B).

Degradation of mutant SOD1 by Dorfin-CHIP chimeric proteins

To assess the degradation activity of Dorfin-CHIP^{L} against mutant SOD1s, we performed the pulse-chase analysis on N2a

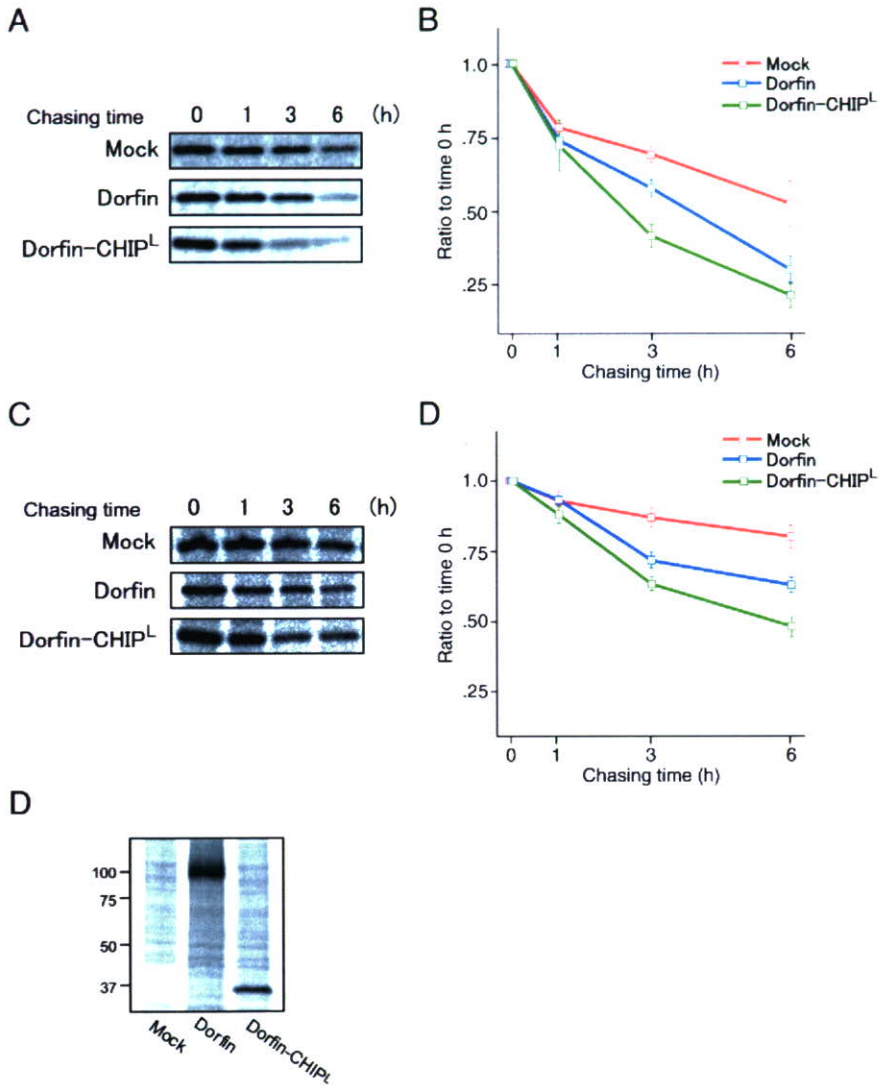

Fig. 6. Degradation of mutant SOD1 proteins with Dorfin-CHIP^{L}. (A) Pulse-chase analysis of SOD1^{G85R} with Dorfin-CHIP^{L}. N2a cells were coexpressed with SOD1^{G85R}-Myc and Mock, Dorfin, and Dorfin-CHIP^{L}. Pulse-chase experiments using [^{35}S]-Met/Cys were done. Immunoprecipitation using anti-Myc antibody and SOD-PAGE analysis revealed the degradation speed of SOD1^{G85R}-Myc. (B) Serial changes in the amount of SOD1^{G85R} coexpressed with Mock, Dorfin, or Dorfin-CHIP^{L}. Four independent experiments were performed and the amounts of SOD1^{G85R} were plotted. There were significant differences between Mock and Dorfin ($p<0.005$), Mock and Dorfin-CHIP^{L} ($p<0.005$), and Dorfin and Dorfin-CHIP^{L} ($p<0.05$) at 3 h, as well as between Mock and Dorfin ($p<0.05$), and Mock and Dorfin-CHIP^{L} ($p<0.05$) at 6 h after labeling. Values are the means±SE, $n=4$. Statistical analysis was done by one-way ANOVA. (C) Pulse-chase analysis of SOD1^{G93A} with Dorfin-CHIP^{L}. N2a cells were coexpressed with SOD1^{G93A}-Myc and Mock, Dorfin, and Dorfin-CHIP^{L} as in panel A. (D) Serial changes in the amount of SOD1^{G93A} coexpressed with Mock, Dorfin, or Dorfin-CHIP^{L}. Four independent experiments were performed and the amounts of SOD1^{G93A} were plotted. There were significant differences between Mock and Dorfin ($p<0.05$) and Mock and Dorfin-CHIP^{L} ($p<0.01$) at 3 h, as well as between Mock and Dorfin ($p<0.05$), Mock and Dorfin-CHIP^{L} ($p<0.01$), and Dorfin and Dorfin-CHIP^{L} ($p<0.05$) at 6 h after labeling. Values are the means±SE, $n=4$. Statistics were done by one-way ANOVA. (E) The equivalent protein expression levels of Dorfin and Dorfin-CHIP^{L}. Half of the volume of samples used in the pulse-chase analysis of panel C at 0 h was used for immunoprecipitation using anti-Flag M2 antibody. The following SOD-PAGE analysis revealed the amounts of Dorfin and Dorfin-CHIP^{L} in the experiment shown in panel C.

cells, using [^{35}S] labeled Met/Cys. The protein levels of SOD1^{G85R} and SOD1^{G93A} declined more rapidly with Dorfin coexpression. Dorfin-CHIP^{L} remarkably declined in both SOD1^{G85R} and SOD1^{G93A} (Figs. 6A, C). Dorfin and Dorfin-CHIP^{L} had similar expression levels at 0 h of this experiment (Fig. 6E). As compared to Mock, Dorfin showed significant declines of both SOD1^{G85R} at 3 h ($p<0.001$) and 6 h ($p<0.05$) after labeling, as shown in a previous study (Niwa et al., 2002). Dorfin-CHIP^{L} also significantly accelerated the decline of SOD1^{G85R} at 3 h ($p<0.001$) and 6 h ($p<0.05$) after labeling again as compared to Mock. At 3 h after labeling, a significant difference between Dorfin-CHIP^{L} and Dorfin was present with respect to SOD1^{G85R} degradation ($p<0.05$). As compared to Dorfin, Dorfin-CHIP^{L} also tended toward accelerated SOD1^{G85R} degradation at 6 h after labeling (Fig. 6B). Similarly, Dorfin showed significant declines of SOD1^{G93A} at 3 h ($p<0.05$) and 6 h ($p<0.05$) after labeling, and Dorfin-CHIP^{L} significantly accelerated the declines of SOD1^{G93A} at 3 h ($p<0.01$) and 6 h ($p<0.01$) after labeling as compared to Mock. A significant difference between Dorfin-CHIP^{L} and Dorfin was present at 6 h in SOD1^{G93A} degradation ($p<0.05$) (Fig. 6D).

Attenuation of the toxicity of mutant SOD1 and decrease in the formation of visible aggregations of mutant SOD1 in cultured neuronal culture cells

The ability of Dorfin-CHIP chimeric proteins to attenuate mutant SOD1-related toxicity was analyzed by MTS assay using N2a cells. The expression of SOD1^{G85R}, as compared to that of SOD1^{WT}, decreased the viability of cells. Overexpression of Dorfin reversed the toxic effect of SOD1^{G85R}, whereas overexpression of CHIP did not. Dorfin-CHIP^{L} had a significantly greater rescue effect on SOD1^{G85R}-related cell toxicity than did Dorfin (Fig. 7A). We also measured the cell viability of N2a cells overexpressing Mock, Dorfin, and Dorfin-CHIP^{L} with various amounts of constructs, and found no difference in toxicity among them (Supplementary Fig. 2).

A structure that Johnston et al. (1998) called aggresome is formed when the capacity of a cell to degrade misfolded proteins is exceeded. The accumulation of mutant SOD1 induces visible macroaggregation, which is considered to be 'aggresome' in N2a cells. We examined the subcellular localizations of Dorfin, CHIP, and Dorfin-CHIP^{L} by immunostaining N2a cells expressing SOD1^{G85R}-GFP. Dorfin was localized in aggresomes with substrate proteins, as in our previous studies. Dorfin-CHIP^{L} was also seen in aggresomes, whereas the staining of CHIP was diffusely observed in the cytosol (Fig. 7B). We counted these visible aggregations with or without MG132 treatment. Dorfin decreased the number of aggregation-containing cells, as has been reported (Niwa et al., 2002), but Dorfin-CHIP^{L} did so more effectively. These effects were inhibited by the treatment of MG132 (Fig. 7C).

Discussion

E3 proteins can specifically recognize and degrade accumulating aberrant proteins, which are deeply involved in the pathogenesis of neurodegenerative disorders, including ALS (Alves-Rodrigues et al., 1998; Sherman and Goldberg, 2001; Ciechanover and Brundin, 2003). For this reason, E3 proteins are candidate molecules for use in developing therapeutic technology for neurodegenerative diseases. Dorfin is the first E3 molecule that has been found specifically to ubiquitylate mutant SOD1 proteins as well as to attenuate mutant SOD-associated toxicity in cultured neuronal cells (Niwa et al., 2002).

NEDL1, a HECT type E3 ligase, has also been reported to be a mutant SOD1-specific E3 ligase and to interact with TRAPδ and dvl1 (Miyazaki et al., 2004). It has also been reported that ubiquitylation of mutant SOD1-associated complex was enhanced by CHIP and Hsp70 *in vivo* (Urushitani et al., 2004). CHIP ubiquitylated Hsp70-holding SOD1 complexes and degraded mutant SOD1, but did not directly interact with mutant SOD1 (Urushitani et al., 2004). Among these E3 molecules, Dorfin seems to be the most potentially beneficial E3 protein for use in ALS therapy since it is the only one that has been demonstrated to reverse mutant SOD1-associated toxicity (Niwa et al., 2002). Furthermore, Dorfin has been localized in various ubiquitin-positive inclusions such as Lewy bodies (LB) in PD, as well as LB-like inclusions in sporadic ALS and glial cell bodies in multiple-system atrophy. These findings indicate that Dorfin may be involved in the pathogenesis of a broad spectrum of neurodegenerative disorders other than familial ALS (Hishikawa et al., 2003; Ito et al., 2003; Ishigaki et al., 2004).

The half-life of Dorfin^{WT} is, however, less than 1 h (Fig. 1, Table 1). The amount of Dorfin is increased in the presence of MG132, a proteasome inhibitor, indicating that Dorfin is immediately degraded in the UPS. Since the nonfunctional RING mutant form of Dorfin, Dorfin$^{C132S/C135S}$, degraded more slowly than did Dorfin^{WT}, Dorfin seemed to be degraded by auto-ubiquitylation. The degradation of Dorfin$^{C132S/C135S}$ is also inhibited by MG132, suggesting that it is degraded by endogenous Dorfin or other E3s. This immediate degradation of Dorfin is a serious problem for its therapeutic application against neurodegenerative diseases.

Several reports have shown that engineered chimera E3s are able to degrade certain substrates with high efficiency. Protac, a chimeric protein-targeting molecule, was designed to target methionine aminopeptidase-2 to Skp1-Cullin-F box complex (SCF) ubiquitin ligase complex for ubiquitylation and degradation (Sakamoto et al.,

Fig. 7. Dorfin-CHIP chimeric proteins can attenuate toxicity induced by mutant SOD1 and decrease the formation of visible aggregation of mutant SOD1 in N2a cells. (A) N2a cells were grown in 96 collagen-coated wells (5000 cells per well) and transfected with 0.15 μg of SOD1^{WT} and 0.05 μg of Mock or 0.15 μg of SOD1^{G85R} and 0.05 μg of Mock, Dorfin, CHIP, or Dorfin-CHIP^{L}. After the medium was changed, MTS assays were done at 48 h of incubation. Viability was measured as the level of absorbance (490 nm). Values are the means±SE, $n=6$. Statistics were carried out by one-way ANOVA. There were significant differences between SOD1^{G85R}-expressing cells coexpressed with Mock and SOD1^{G85R}-expressing cells coexpressed with Dorfin ($p<0.001$), as well as between SOD1^{G85R}-expressing cells coexpressed with Dorfin and SOD1^{G85R}-expressing cells coexpressed with Dorfin-CHIP^{L} ($p<0.001$). (B) N2a cells were transiently expressed with SOD1^{G85R}-GFP and Mock, Dorfin, CHIP, or Dorfin-CHIP^{L}. Immunostaining with anti-FLAG antibody revealed that Dorfin, CHIP, and Dorfin-CHIP^{L} were localized with SOD1^{G85R}-GFP in macroaggresomes (arrows). Scale bar=20 μm (C) The visible macroaggregations in N2a cells expressing both SOD1^{G85R}-GFP and Mock, Dorfin, CHIP, or Dorfin-CHIP^{L} with or without MG132 treatment were counted and the ratio of cells with aggregations to those with GFP signals was calculated. Values are the means±SE, $n=4$. Statistics were done by one-way ANOVA. *$p<0.01$ denotes a significant difference between cells with Mock and Dorfin or Dorfin-CHIP^{L}. **$p<0.05$ denotes a significant difference between cells with Dorfin and Dorfin-CHIP^{L}.

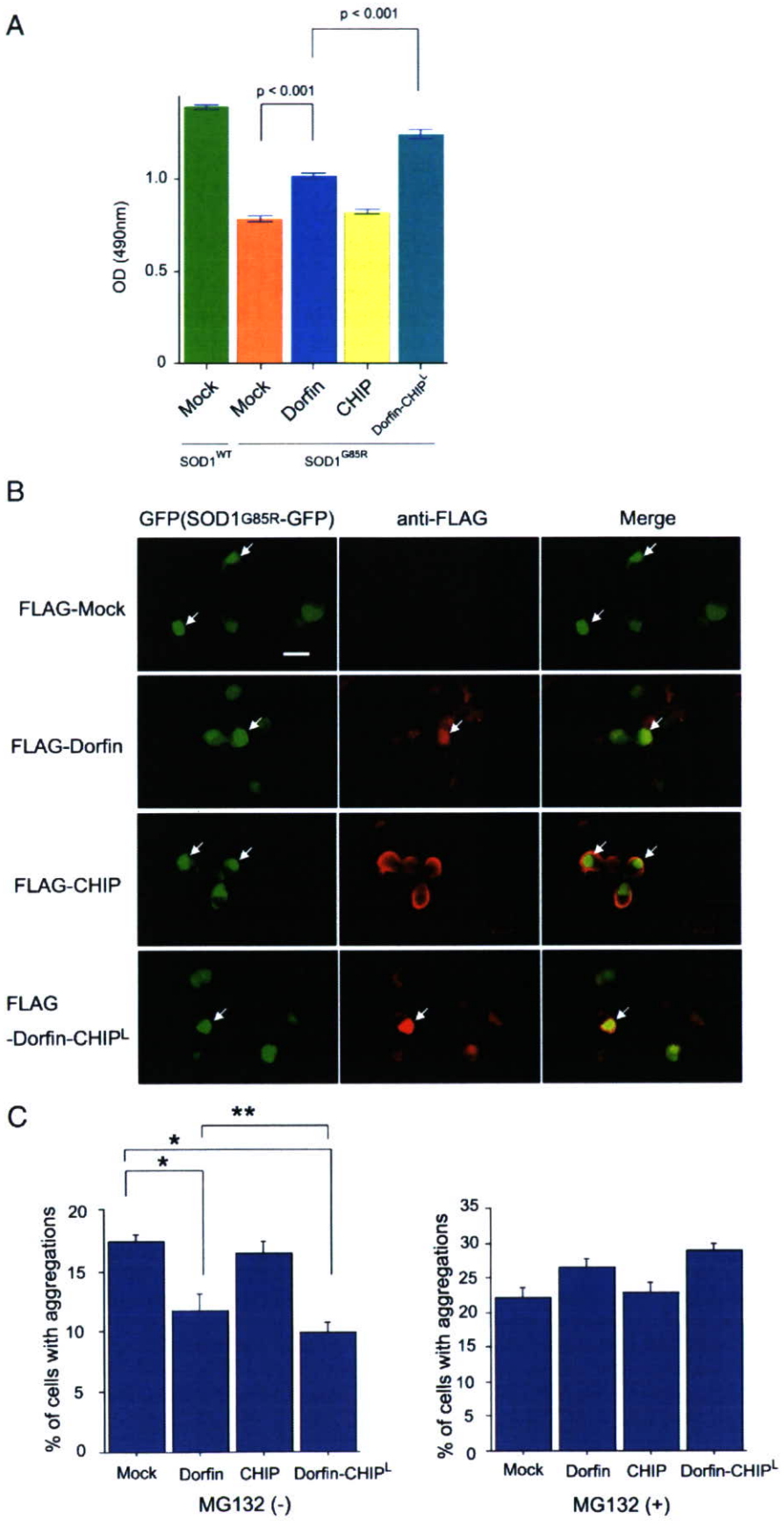
A
p < 0.001
p < 0.001
OD (490nm)
1.0
0.5
0
Mock
Mock
Dorfin
CHIP
Dorfin-CHIP^L
SOD1^WT
SOD1^G85R
B
GFP(SOD1G85R-GFP)
anti-FLAG
Merge
FLAG-Mock
FLAG-Dorfin
FLAG-CHIP
FLAG
-Dorfin-CHIP^L
C
**
*
*
% of cells with aggregations
20
15
10
5
0
Mock
Dorfin
CHIP
Dorfin-CHIP^L
MG132 (-)
35
30
25
20
15
10
5
0
MG132 (+)

2001, 2003). Oyake et al. (2002) developed double RING ubiquitin ligases containing the RING finger domains of both BRCA and BARD1 linked to a substrate recognition site PCNA. Recently, Hatakeyama et al. developed a fusion protein composed of Max, which forms a heterodimer with c-Myc, and the U-box of CHIP. This fusion protein physically interacted with c-Myc and promoted the ubiquitylation of c-Myc. It also reduced the stability of c-Myc, resulting in the suppression of transcriptional activity dependent on c-Myc and the inhibition of tumorogenesis (Hatakeyama et al., 2005). This indicated that the U-box portion of CHIP is able to add an effective E3 function to a U-box-containing client protein.

We postulated that engineered forms of Dorfin could be stable and still function as specific E3s for mutant SOD1s. Dorfin has a RING/IBR domain in the N-terminal portion (amino acids 1-332), but has no obvious motif in the rest of the C-terminus (amino acids 333–838). In this study, we have demonstrated that the hydrophobic domain of Dorfin (amino acids 333–454) is both necessary and sufficient for substrate recruiting (Fig. 2B). In our engineered proteins, the RING/IBR motif of N-terminal Dorfin was replaced by the UPR domain of CHIP, which had strong E3 activity (Murata et al., 2001). Some of the engineered Dorfin-chimeric proteins, such as Dorfin-CHIP$^{D, G, J}$, and ^{L}, were degraded *in vivo* far more slowly than was wild-type Dorfin, indicating that they were capable of being stably presented *in vivo* (Fig. 3). However, Dorfin-CHIP^{G} failed to show strong ubiquitylation activity against SOD1^{G85R} in HEK293 cells. Since Dorfin-CHIP$^{D, J}$, and ^{L} were able to bind to SOD1^{G85R} more strongly than did Dorfin-CHIP^{G}, the binding activity was more important for the E3 activity than for the protein stability.

We next showed that although all of the Dorfin-CHIP chimeric proteins bound to mutant SOD1 *in vivo*, some of them, such as Dorfin-CHIP$^{B, C}$, and ^{I}, bound less than others (Fig. 4A). In HEK293 cells, Dorfin-CHIP$^{D, E, F, J, K}$, and ^{L} ubiquitylated SOD1^{G85R} more effectively than did Dorfin or CHIP; however, in N2a cells only Dorfin-CHIP^{L} had more effective E3 activity than did Dorfin or CHIP. This discrepancy may be due to differences between HEK 293 and N2a cells which could provide slight different environment for the E3 machinery. Therefore, Dorfin-CHIP^{L} was the most potent of the candidate chimeric proteins in degrading mutant SOD1 in the UPS in neuronal cells. We also showed that Dorfin-CHIP^{L} could specifically bind to and ubiquitylate mutant SOD1s but not SOD1^{WT} *in vivo*, as Dorfin had done (Niwa et al., 2002; Ishigaki et al., 2004) (Fig. 5). This observation confirmed that the hydrophobic domain of Dorfin (amino acids 333–454) is responsible for mutant SOD1 recruiting.

Pulse-chase analysis using N2a cells showed that Dorfin-CHIP^{L} degraded SOD1^{G85R} and SOD1^{G93A} more effectively than did Dorfin (Fig. 6). This is compatible with the finding that Dorfin-CHIP^{L} had a greater effect than Dorfin did on the ubiquitylation against mutant SOD1. The cycloheximide assay verified that the degradation ability of Dorfin-CHIP^{L} against SOD1^{G85R} was stronger than that of Dorfin or CHIP in HEK293 cells (data not shown).

Dorfin-CHIP^{L} also reversed SOD1^{G85R}-associated toxicity in N2a cells more effectively than did Dorfin (Fig. 7). This therapeutic effect of Dorfin-CHIP^{L} was expected from its strong E3 activity and degradation ability against SOD1^{G85R}. Visible protein aggregations have been considered to be hallmarks of neurodegeneration. Increased understanding of the pathway involved in protein aggregation may demonstrate that visible macroaggregates represent the end-stage of a molecular cascade of steps rather than a direct toxic insult (Ross and Poirier, 2004). Two facts that Dorfin-CHIP^{L} decreased aggregation formation of SOD1^{G85R} and that this effect was inhibited by a proteasome inhibitor should reflect the ability of Dorfin-CHIP^{L} to degrade mutant SOD1 in the UPS of cells.

Based on our present observations, Dorfin-CHIP^{L}, an engineered chimeric molecule with the hydrophobic substrate-binding domain of Dorfin and the U-box domain of CHIP, had stronger E3 activity against mutant SOD1 than did Dorfin or CHIP. Indeed, it not only degraded mutant SOD1 more effectively than did Dorfin or CHIP but, as compared to Dorfin, produced marked attenuation of mutant SOD1-associated toxicity in N2a cells. This protective effect of Dorfin-CHIP^{L} against mutant SOD1 has potential applications to gene therapy for mutant SOD1 transgenic mice because this protein has a long enough life to allow the constant removal of mutant SOD1 from neurons. Since Dorfin was originally identified as a sporadic ALS-associated molecule (Ishigaki et al., 2002b) and is located in the ubiquitin-positive inclusions of various neurodegenerative diseases (Hishikawa et al., 2003), this molecule is an appropriate candidate for future use in gene therapy not only for familial ALS, but also for sporadic ALS and other neurodegenerative disorders.

So far, most reports on engineered chimera E3s have targeted cancer-promoting proteins. Dorfin-CHIP chimeric proteins are the first chimera E3s to be intended for the treatment of neurodegenerative diseases. Since the accumulation of ubiquitylated proteins in neurons is a pathological hallmark of various neurodegenerative diseases, development of chimera E3s like Dorfin-CHIP^{L}, which can remove unnecessary proteins, is a new therapeutic concept. Further analysis, including transgenic overexpression and vector delivery of Dorfin-CHIP chimeric proteins using ALS animal models will increase our understanding of the potential utility of Dorfin-CHIP chimeric proteins as therapeutic tools.

Acknowledgments

We gratefully thank Dr. Shigetsugu Hatakeyama at Hokkaido University for his advice about the construction of Dorfin-CHIP chimeric proteins. This work was supported by the Nakabayashi Trust for ALS Research; a grant for Center of Excellence (COE) from the Ministry of Education, Culture, Sports, Science and Technology of Japan; and grants from the Ministry of Health, Welfare and Labor of Japan.

Appendix A. Supplementary data

Supplementary data associated with this article can be found, in the online version, at doi:10.1016/j.nbd.2006.09.017.

References

Alves-Rodrigues, A., Gregori, L., Figueiredo-Pereira, M.E., 1998. Ubiquitin, cellular inclusions and their role in neurodegeneration. Trends Neurosci. 21, 516–520.

Bercovich, B., Stancovski, I., Mayer, A., Blumenfeld, N., Laszlo, A., Schwartz, A.L., Ciechanover, A., 1997. Ubiquitin-dependent degradation of certain protein substrates in vitro requires the molecular chaperone Hsc70. J. Biol. Chem. 272, 9002–9010.

Ciechanover, A., Brundin, P., 2003. The ubiquitin proteasome system in

neurodegenerative diseases: sometimes the chicken, sometimes the egg. Neuron 40, 427–446.

Cudkowicz, M.E., McKenna-Yasek, D., Sapp, P.E., Chin, W., Geller, B., Hayden, D.L., Schoenfeld, D.A., Hosler, B.A., Horvitz, H.R., Brown, R.H., 1997. Epidemiology of mutations in superoxide dismutase in amyotrophic lateral sclerosis. Ann. Neurol. 41, 210–221.

Glickman, M.H., Ciechanover, A., 2002. The ubiquitin–proteasome proteolytic pathway: destruction for the sake of construction. Physiol. Rev. 82, 373–428.

Hatakeyama, S., Matsumoto, M., Kamura, T., Murayama, M., Chui, D.H., Planel, E., Takahashi, R., Nakayama, K.I., Takashima, A., 2004. U-box protein carboxyl terminus of Hsc70-interacting protein (CHIP) mediates poly-ubiquitylation preferentially on four-repeat Tau and is involved in neurodegeneration of tauopathy. J. Neurochem. 91, 299–307.

Hatakeyama, S., Watanabe, M., Fujii, Y., Nakayama, K.I., 2005. Targeted destruction of c-Myc by an engineered ubiquitin ligase suppresses cell transformation and tumor formation. Cancer Res. 65, 7874–7879.

Hishikawa, N., Niwa, J., Doyu, M., Ito, T., Ishigaki, S., Hashizume, Y., Sobue, G., 2003. Dorfin localizes to the ubiquitylated inclusions in Parkinson's disease, dementia with Lewy bodies, multiple system atrophy, and amyotrophic lateral sclerosis. Am. J. Pathol. 163, 609–619.

Ishigaki, S., Liang, Y., Yamamoto, M., Niwa, J., Ando, Y., Yoshihara, T., Takeuchi, H., Doyu, M., Sobue, G., 2002a. X-Linked inhibitor of apoptosis protein is involved in mutant SOD1-mediated neuronal degeneration. J. Neurochem. 82, 576–584.

Ishigaki, S., Niwa, J., Ando, Y., Yoshihara, T., Sawada, K., Doyu, M., Yamamoto, M., Kato, K., Yotsumoto, Y., Sobue, G., 2002b. Differentially expressed genes in sporadic amyotrophic lateral sclerosis spinal cords—Screening by molecular indexing and subsequent cDNA microarray analysis. FEBS Lett. 531, 354–358.

Ishigaki, S., Hishikawa, N., Niwa, J., Iemura, S., Natsume, T., Hori, S., Kakizuka, A., Tanaka, K., Sobue, G., 2004. Physical and functional interaction between Dorfin and Valosin-containing protein that are colocalized in ubiquitylated inclusions in neurodegenerative disorders. J. Biol. Chem. 279, 51376–51385.

Ito, T., Niwa, J., Hishikawa, N., Ishigaki, S., Doyu, M., Sobue, G., 2003. Dorfin localizes to Lewy bodies and ubiquitylates synphilin-1. J. Biol. Chem. 278, 29106–29114.

Johnston, J.A., Ward, C.L., Kopito, R.R., 1998. Aggresomes: a cellular response to misfolded proteins. J. Cell Biol. 143, 1883–1898.

Julien, J.P., 2001. Amyotrophic lateral sclerosis. unfolding the toxicity of the misfolded. Cell 104, 581–591.

Jungmann, J., Reins, H.A., Schobert, C., Jentsch, S., 1993. Resistance to cadmium mediated by ubiquitin-dependent proteolysis. Nature 361, 369–371.

Lee, D.H., Sherman, M.Y., Goldberg, A.L., 1996. Involvement of the molecular chaperone Ydj1 in the ubiquitin-dependent degradation of short-lived and abnormal proteins in *Saccharomyces cerevisiae*. Mol. Cell. Biol. 16, 4773–4781.

Meacham, G.C., Patterson, C., Zhang, W., Younger, J.M., Cyr, D.M., 2001. The Hsc70 co-chaperone CHIP targets immature CFTR for proteasomal degradation. Nat. Cell Biol. 3, 100–105.

Miyazaki, K., Fujita, T., Ozaki, T., Kato, C., Kurose, Y., Sakamoto, M., Kato, S., Goto, T., Itoyama, Y., Aoki, M., Nakagawara, A., 2004. NEDL1, a novel ubiquitin–protein isopeptide ligase for dishevelled-1, targets mutant superoxide dismutase-1. J. Biol. Chem. 279, 11327–11335.

Murata, S., Minami, Y., Minami, M., Chiba, T., Tanaka, K., 2001. CHIP is a chaperone-dependent E3 ligase that ubiquitylates unfolded protein. EMBO Rep. 2, 1133–1138.

Murata, S., Chiba, T., Tanaka, K., 2003. CHIP: a quality-control E3 ligase collaborating with molecular chaperones. Int. J. Biochem. Cell Biol. 35, 572–578.

Niwa, J., Ishigaki, S., Doyu, M., Suzuki, T., Tanaka, K., Sobue, G., 2001. A novel centrosomal ring-finger protein, dorfin, mediates ubiquitin ligase activity. Biochem. Biophys. Res. Commun. 281, 706–713.

Niwa, J., Ishigaki, S., Hishikawa, N., Yamamoto, M., Doyu, M., Murata, S., Tanaka, K., Taniguchi, N., Sobue, G., 2002. Dorfin ubiquitylates mutant SOD1 and prevents mutant SOD1-mediated neurotoxicity. J. Biol. Chem. 277, 36793–36798.

Oyake, D., Nishikawa, H., Koizuka, I., Fukuda, M., Ohta, T., 2002. Targeted substrate degradation by an engineered double RING ubiquitin ligase. Biochem. Biophys. Res. Commun. 295, 370–375.

Rosen, D.R., Siddique, T., Patterson, D., Figlewicz, D.A., Sapp, P., Hentati, A., Donaldson, D., Goto, J., O'Regan, J.P., Deng, H.X., et al., 1993. Mutations in Cu/Zn superoxide dismutase gene are associated with familial amyotrophic lateral sclerosis. Nature 362, 59–62.

Ross, C.A., Poirier, M.A., 2004. Protein aggregation and neurodegenerative disease. Nat. Med. 10, S10–S17 (Suppl.).

Rowland, L.P., Shneider, N.A., 2001. Amyotrophic lateral sclerosis. N. Engl. J. Med. 344, 1688–1700.

Sakamoto, K.M., Kim, K.B., Kumagai, A., Mercurio, F., Crews, C.M., Deshaies, R.J., 2001. Protacs: chimeric molecules that target proteins to the Skp1-Cullin-F box complex for ubiquitination and degradation. Proc. Natl. Acad. Sci. U. S. A. 98, 8554–8559.

Sakamoto, K.M., Kim, K.B., Verma, R., Ransick, A., Stein, B., Crews, C.M., Deshaies, R.J., 2003. Development of Protacs to target cancer-promoting proteins for ubiquitination and degradation. Mol. Cell Proteomics 2, 1350–1358.

Scheffner, M., Nuber, U., Huibregtse, J.M., 1995. Protein ubiquitination involving an E1–E2–E3 enzyme ubiquitin thioester cascade. Nature 373, 81–83.

Sherman, M.Y., Goldberg, A.L., 2001. Cellular defenses against unfolded proteins: a cell biologist thinks about neurodegenerative diseases. Neuron 29, 15–32.

Shimura, H., Schwartz, D., Gygi, S.P., Kosik, K.S., 2004. CHIP–Hsc70 complex ubiquitinates phosphorylated tau and enhances cell survival. J. Biol. Chem. 279, 4869–4876.

Tanaka, K., Suzuki, T., Hattori, N., Mizuno, Y., 2004. Ubiquitin, proteasome and parkin. Biochim. Biophys. Acta 1695, 235–247.

Urushitani, M., Kurisu, J., Tateno, M., Hatakeyama, S., Nakayama, K., Kato, S., Takahashi, R., 2004. CHIP promotes proteasomal degradation of familial ALS-linked mutant SOD1 by ubiquitinating Hsp/Hsc70. J. Neurochem. 90, 231–244.

Yoshida, Y., Tokunaga, F., Chiba, T., Iwai, K., Tanaka, K., Tai, T., 2003. Fbs2 is a new member of the E3 ubiquitin ligase family that recognizes sugar chains. J. Biol. Chem. 278, 43877–43884.

Gene Expression Profiling toward Understanding of ALS Pathogenesis

FUMIAKI TANAKA, JUN-ICHI NIWA, SHINSUKE ISHIGAKI, MASAHISA KATSUNO, MASAHIRO WAZA, MASAHIKO YAMAMOTO, MANABU DOYU, AND GEN SOBUE

Department of Neurology, Nagoya University Graduate School of Medicine, 65 Tsurumai-cho, Showa-ku, Nagoya 466-8550, Japan

ABSTRACT: **Although more than 130 years have gone by since the first description in 1869 by Jean-Martin Charcot, the mechanism underlying the characteristic selective motor neuron degeneration in amyotrophic lateral sclerosis (ALS) has remained elusive. Modest advances in this research field have been achieved by the identification of copper/zinc superoxide dismutase 1 (SOD1) as one of the causative genes for rare familial ALS (FALS) and by the development and analysis of mutant SOD1 transgenic mouse models. However, in sporadic ALS (SALS) with many more patients, causative or critical genes situated upstream of the disease pathway have not yet been elucidated and no available disease models have been established. To approach genes causative or critical for ALS, gene expression profiling in tissues primarily affected by the disease has represented an attractive research strategy. We have been working on screening these genes employing and combining several new technologies such as cDNA microarray, molecular indexing, and laser capture microdissection. Many of the resultant genes are of intense interest and may provide a powerful tool for determining the molecular mechanisms of ALS. However, we have barely arrived at the starting point and are confronting an enormous number of genes whose roles remain undetermined. Challenging tasks lie ahead of us such as identifying which genes are really causative for ALS and developing a disease model of SALS with due consideration for the expression changes in those genes.**

KEYWORDS: **ALS; SOD1; gene expression analysis; cDNA microarray; molecular indexing; laser capture microdissection**

INTRODUCTION

Amyotrophic lateral sclerosis (ALS) is a neurodegenerative and fatal human disorder characterized by loss of motor neurons in the spinal cord, brain stem,

Address for correspondence: Dr. Gen Sobue, Department of Neurology, Nagoya University Graduate School of Medicine, 65 Tsurumai-cho, Showa-ku, Nagoya 466-8550, Japan. Voice: +81-52-744-2385; fax: +81-52-744-2384.
e-mail: sobueg@med.nagoya-u.ac.jp

Ann. N.Y. Acad. Sci. 1086: 1–10 (2006).
doi: 10.1196/annals.1377.011

and motor cortex, presenting as weakness of the limbs, speech abnormalities, and difficulties in swallowing.[1] The terminal phases of the disease involve respiratory insufficiency and half of the patients die within 3 years after the onset of symptoms. ALS can be inherited as an autosomal dominant trait in a subset of individuals who make up 5% to 10% of the total population of those affected. In addition, 20% to 30% of familial ALS (FALS) cases are associated with a mutation in the copper/zinc superoxide dismutase 1 gene (SOD1).[2] However, more than 90% of ALS patients are sporadic, not showing any familial trait. Since there have been no available disease models for sporadic ALS (SALS) as of now, transgenic mouse models or cell culture models[3] of ALS associated with SOD1 mutations have proven very useful in studying the initial mechanisms underlying this neurodegenerative disease of unknown etiology. The use of an animal model makes it possible and easy to investigate the different stages of disease progression including the early preclinical phase.

One of the experimental approaches toward a more comprehensive understanding of the molecular changes occurring in ALS is gene expression study[4] employing array-based methods or a differential display and its related techniques. Using transgenic mouse models expressing the SOD1 gene with a G93A mutation, we performed cDNA microarray analysis[5] to reveal the transcriptional profiles of affected tissues, namely, spinal anterior horn tissues. This analysis revealed an upregulation of genes related to an inflammatory process together with a change in apoptosis-related gene expression at the presymptomatic stage prior to motor neuron death.

Next, we extended our gene expression study from mouse to human postmortem spinal anterior horn tissues obtained from SALS patients. In this analysis, we employed a molecular indexing technique, a modified version of the differential display developed by Kato in 1995.[6] These PCR-based screening procedures have the advantage of being able to cover an unrestricted range of expressed genes including even hitherto unknown ones. As a result, we have successfully cloned a novel gene designated "dorfin,"[7] the expression of which was upregulated in SALS spinal cords.

Using spinal anterior horn tissues of SOD1 mutant mice or SALS patients as starting materials, these gene expression studies[5,7] have shed considerable light on the pathogenesis of FALS and SALS. However, in the spinal anterior horn tissues of ALS spinal cords, there are reduced numbers of motor neurons with glial cell proliferation. The alteration of the gene expression in the spinal anterior horn tissues could reflect the number of motor neurons and glial cells during disease progression. Such a disadvantage in using anterior horn tissues as starting materials prompted us to try to extract a pure motor neuron-specific gene expression profile. To this end, we employed the technology of laser capture microdissection[8] combined with T7-based RNA amplification and cDNA microarrays, which culminated in the successful detection of a total of 196 genes considered important for the SALS molecular mechanism.[9]

GENE EXPRESSION ANALYSIS FOR MUTANT SOD1 MOUSE MODEL OF ALS

We analyzed both temporal and differential gene expressions in the lumbar spinal anterior horn tissues of the transgenic mouse models expressing the SOD1 gene with a G93A mutation and the controls.[5] In this analysis, we detected a significant upregulation of 30 specific transcripts and downregulation of 7 transcripts in the spinal cords of mutant SOD1 mice[5] (TABLE 1). Before 11 weeks of age, mutant SOD1 mice are free of a disease phenotype, but they begin to decline rapidly in motor function after 14 weeks. The employment of mice for gene expression analysis provides a great advantage in obtaining data in the preclinical stage.

Interestingly, we found an upregulation of genes related to an inflammatory process together with a change in apoptosis-related gene expression at 11 weeks of age in the preclinical stage prior to motor neuron death.[5] The representative inflammatory-related genes elevated in their expression at this stage were the tumor necrosis factor (TNF)-α gene, which is a proinflammatory cytokine, and the Janus tyrosine-protein kinase 3 (JAK3), a necessary component of cytokine receptor signaling (TABLE 1). At a subsequent disease stage of 14 or 17 weeks of age, many more genes associated with an inflammatory process such as cathepsin D, serine protease inhibitor (SPI) 2–4, and cystatin C precursor, CD68, CD147, and clusterin increased their expression (TABLE 1). A histopathological evaluation showed glial cell activation and proliferation as early as 11 weeks of age and continuing to advance until 17 weeks.[10] A temporal increase in the expression level observed in these genes might reflect an inflammatory response with activated microglia and reactive astrocytes.

On the other hand, caspase-1, an initiator of the neuronal apoptotic cascade, was also upregulated at a presymptomatic 11 weeks of age (TABLE 1). An interrelationship between the inflammatory reaction and apoptotic pathway has been demonstrated. In addition to its role as an initiator of neuronal apoptotis, extracellular caspase-1 converts interleukin-1β (IL-1β) into a mature form. Thus, caspase-1 activation in motor neurons contributes to an inflammatory pathway with early astrocytosis and microglial activation in mutant SOD1 mice. In contrast, there is strong evidence for an inflammatory response involving microglial activation that leads to neuronal apoptosis.[11] Activated microglia express neurotoxic cytokines and substances such as TNF-α, proteases, oxyradicals, and small reactive molecules.[12] A nearly simultaneous upregulation of genes related to an inflammatory process and apoptotic initiation at the preclinical stage might contribute to the relentless neurodegenerative process making for a detrimental cycle. At 14 weeks of age, an early phase of the symptomatic stage, a key executioner of apoptosis, caspase-3, resulting from caspase-1 activation, began to be upregulated.[13] This finding agrees with

TABLE 1. Differentially expressed predominant genes detected in spinal anterior horn or spinal motor neurons from SOD1 mutant mice and sporadic ALS patients

Analysis object	SOD1 G93A mutant mice[5,13] spinal anterior horn	SALS patients[7,18] spinal anterior horn	SALS patients[9] spinal anterior horn	SALS patients[9] spinal motor neuron
Analysis method	cDNA microarray	Molecular indexing	cDNA microarray	cDNA microarray
Upregulated genes in ALS	30/1176	46/entire mRNA	37/4845	52/4845
	TNF-α*†	dorfin*	KIAA0231	death receptor 5 (DR5)*
	JAK3†	TAFII30*	fibrinogen A a polypeptide	cyclin A1, cyclin C*, ephrin A1*
	cathepsin D	neugrin*	presenilin 1	caspase 1, caspase 3, caspase 9
	serine protease inhibitor (SPI) 2–4		ephrin A1	acetyl-coenzyme A transporter*, NF-κB
	cystatin C precursor		transcription factor NF-Atc	ciliary neurotrophic factor (CNTF)
	CD68*, CD147		SH3-binding protein 2	hepatocyte growth factor (HGF)
	clusterin		integrin alpha E precursor (ITGAE)	glial cell line-derived neurotrophic factor (GDNF)
	caspase-1*†, caspase-3		cysteine dioxygenase, type 1	KIAA0231*
	GFAP*, vimentin			glutamate receptor subunit 2 (GLUR-2)
	Bcl-xL			interleukin-1 receptor antagonist
	c-fos, junD			TNF receptor-associated factor 6 (TRAF6)
Downregulated genes in ALS	7/1176	38/entire mRNA	8/4845	144/4845
	XIAP	metallothionein-3*	glutamate receptor, metabotropic 6	dynactin 1 (p150)*, TRK-C*, midkine, musashi 1
	$GABA_A$-receptor-α1	MRP8*	cholecystokinin A receptor	microtubule-associated protein 1A, 4
		ubiquitin-like protein 5*	signal recognition particle 14kD	microtubule-associated protein tau
			syntaxin 1B	early growth response 3 (EGR3)*
			sex-determining region Y (SRY)-box 11	BCL2-antagonist/killer 1 (Bak)*
				cellular retinoic acid-binding protein 1 (CRABP1)*
				retinoic acid receptor-α

Principal genes showing expression changes of 3.0-fold increase and 0.3-fold decrease are listed. Fold-change is calculated by dividing the fluorescence signals of each ALS sample by those of control samples.*Gene expression changes were confirmed by other methods such as reverse transcription-polymerase chain reaction (RT-PCR) or *in situ* hybridization.†Genes upregulated in 11-week-old mice.

the result that at 14 weeks of age XIAP mRNA downregulation occurred in the spinal cords of mutant SOD1 mice (TABLE 1) since XIAP is a direct inhibitor of caspase-3, -7, and -9.[14]

DISCOVERY OF NOVEL GENES ASSOCIATED WITH ALS PATHOGENESIS

To identify genes differentially expressed in the anterior horn tissues of the human SALS spinal cord, we adopted molecular indexing, a modified version of the differential display.[6] The entire mRNA population is identified and displayed by 3′ end cDNA fragments generated by class IIS restriction enzyme digestion and PCR.[6] Accordingly, molecular indexing provides a significant advantage in expression analysis for unknown genes. Among 84 fragments differentially expressed in SALS cloned in the first screening procedure, we noticed a fragment with an unknown sequence overexpressed in SALS spinal cords. We cloned it using RACE methods and named it dorfin (double ring-finger protein)[7] (TABLE 1).

Dorfin contains a RING-IBR (in between ring finger) domain at its N terminus and mediated ubiquitin ligase (E3) activity.[7] Interestingly, dorfin is predominantly localized and overexpressed in the ubiquitinated neuronal hyaline inclusion bodies found in the motor neurons of SALS patients as well as FALS patients with a SOD1 mutation and of mutant SOD1-transgenic mice.[15,16] An *in vitro* assay revealed that dorfin physically bound and ubiquitylated various SOD1 mutants and enhanced their degradation, and that its overexpression protected neural cells against the toxic effects of mutant SOD1 and reduced SOD1 inclusions.[15,17] These findings suggest that dorfin, an E3 ligase, may play some protective role in the pathogenesis of FALS and SALS via the ubiquitylation and degradation of its substrates, mutant SOD1, and others yet to be identified.

Besides dorfin, we have detected 30-kDa TATA binding protein-associated factor (TAFII30) and neugrin as upregulated genes in the SALS spinal cord[18] (TABLE 1). On the other hand, metallothionein-3, macrophage-inhibiting factor-related protein-8 (MRP-8) and ubiquitin-like protein 5 were downregulated in their expression[18] (TABLE 1).

MOTOR NEURON-SPECIFIC GENE EXPRESSION PROFILE IN SALS

As noted above, even using spinal anterior horn tissues consisting of heterogeneous cell types including motor neurons and glial cells as starting materials, gene expression studies have successfully shed light on the genes related to the pathogenesis of FALS and SALS.[5,7,18] However, the constitution

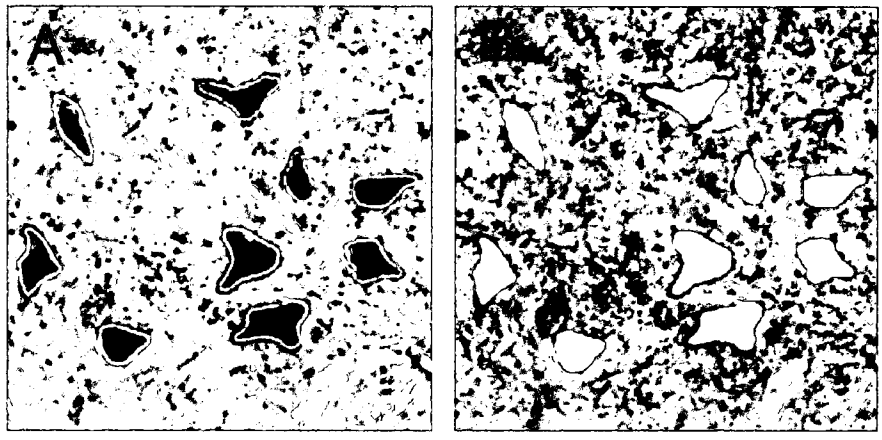

FIGURE 1. Laser microdissection of motor neurons in spinal anterior horn. sections were stained with hematoxylin and margins of motor neurons were dissected by the laser beam (**A**); motor neurons were isolated from slides by laser pressure catapulting (**B**).

of spinal anterior horn tissues is overwhelmingly dominated by glial cells in comparison with motor neurons. Furthermore, in the lesions of ALS spinal cords, there are reduced numbers of motor neurons with glial cell proliferation. When the genes display a dramatic change of expression in ALS motor neurons, they can be detected (TABLE 1) even by using spinal anterior horn tissues. In fact, we have successfully cloned dorfin overexpressed in SALS motor neurons[7] as described above. However, a small change of gene expression in motor neurons might be masked by a large quantity of glial cells and such genes might be those we are seeking as the essential ones for ALS pathomechanisms. The technologies of laser capture microdissection have been developed to provide a reliable method of procuring pure populations of cells from specific microscopic regions of tissue sections under direct visualization.[8,19] The pulsed laser microbeam cut precisely around the targeted motor neurons in the spinal anterior horn (FIG. 1). Each laser-isolated specimen was subsequently transferred to the cap of a PCR tube that was activated by laser pulses.

Using this technology combined with T7 RNA polymerase-based RNA amplification[20] and cDNA microarrays, we have obtained motor neuron-specific gene expression profiles of SALS patients[9] (TABLE 1). Simultaneously, we also conducted conventional gene expression analysis using spinal anterior horn tissues and validated the differential characteristics[9] (TABLE 1). As a result, spinal motor neurons showed a gene expression profile distinct from that of spinal anterior horn tissues (TABLE 1). Of the genes examined 3% (144/4845) were downregulated and 1% (52/4845) were upregulated in motor neurons. Downregulated genes included those associated with cytoskeleton/axonal

transport, transcription, and cell surface antigens/receptors such as dynactin 1, microtubule-associated proteins, and early growth response 3 (EGR3). In contrast, cell death-associated genes were mostly upregulated. Promoters for a cell death pathway, death receptor 5 (DR5), cyclins A1 and C, and caspases-1, -3, and -9, were upregulated as were cell death inhibitors, acetyl-CoA transporter, and NF-κB (TABLE 1). Moreover, neuroprotective neurotrophic factors such as ciliary neurotrophic factor (CNTF), hepatocyte growth factor (HGF), and glial cell line-derived neurotrophic factor (GDNF) were upregulated. However, inflammation-related genes such as those belonging to the cytokine family were not significantly upregulated in SALS motor neurons.

One of the interesting genes downregulated in motor neurons was dynactin 1, recently identified as a causative gene for human motor neuron disease.[21–23] Other motor proteins including the kinesin family responsible for antegrade axonal transport and dyneins for retrograde axonal transport were not changed significantly, but the expression levels of microtubule-associated proteins (MAPs) 1A, 4, and tau were reduced (TABLE 1). The impairment of axonal transport is thought to be an early event in motor neuron degeneration, and the protein levels of MAPs 1A and tau have especially been reported to decrease well before the onset of symptoms in mutant SOD1 transgenic mice also.[24]

As shown in the examples of MAPs 1A and tau, gene expression profiles of SALS patients may share some features with those of SOD1 mutant mice. However, taking into account our overall differential gene expression profiles between mice and humans drawn from spinal anterior horn tissues (TABLE 1), the disease in transgenic mouse may mimic but not be identical to the pathophysiology in human SALS. Consequently, we should be cautious about applying the research results of the pathophysiological process or therapeutic strategy obtained from SOD1 mutant mice to human SALS patients.

Seen in this light, the gene expression data of SALS motor neurons obtained by our analysis are of particular value and contribute a starting point for clarifying the pathomechanisms of a great many more SALS than FALS. At present, it is not easy to determine the genes of primary pathological significance from a total of 144 downregulated and 52 upregulated genes in SALS motor neurons. The primary molecular events should occur in the preclinical phase of the disease. Unlike the case of mice, it is impossible to obtain human spinal cord specimens at a preclinical stage. However, even in postmortem tissue, some motor neurons remain intact and have not yet started to degenerate. From this standpoint, a detailed investigation of the gene expression level, particularly in motor neurons, verified to be intact by reliable neurodegenerative markers would lead to the successful detection of genes related to primary molecular events. Detecting such genes would provide a first step toward a new molecular targeted therapy for SALS by developing animal or cell models mimicking those upstream and primary molecular events determined in human SALS patients.

INTEGRATED RESEARCH FOR NEURODEGENERATION AND TUMORIGENESIS

Among the genes in which we have detected an alteration in their expression in SOD1 mutant mice or SALS patients, a number of them are well known to be related to tumorigenesis rather than neurodegeneration (TABLE 1). Evidence has been steadily accumulating for the existence of many common molecular pathways between neurodegeneration and tumorigenesis.[25] Based on the concept of "Integrated Molecular Medicine for Neuronal and Neoplastic Disorders" proposed by The 21st Century Center of Excellence (COE) Program at Nagoya University,[26] the contribution of these tumor-related genes to the molecular mechanism of ALS should be clarified to advance our understanding of this devastating disease.

ACKNOWLEDGMENTS

We thank Ms. Mikiko Sato and Ms. Yoriko Hiranuma for their help in editing this manuscript and daily management of COE office. This study was supported by The 21st Century COE Program "Integrated Molecular Medicine for Neuronal and Neoplastic Disorders," and the grant from Ministry of Education, Culture, Sports, Science, and Technology of Japan.

REFERENCES

1. INCE, P.G., J. LOWE & P.J. SHAW. 1998. Amyotrophic lateral sclerosis: current issues in classification, pathogenesis and molecular pathology. Neuropathol. Appl. Neurobiol. **24:** 104–117.
2. SIDDIQUE, T. & H.X. DENG. 1996. Genetics of amyotrophic lateral sclerosis. Hum. Mol. Genet. **5:** 1465–1470.
3. TAKEUCHI, H., Y. KOBAYASHI, S. ISHIGAKI, *et al.* 2002. Mitochondrial localization of mutant superoxide dismutase 1 triggers caspase-dependent cell death in a cellular model of familial amyotrophic lateral sclerosis. J. Biol. Chem. **277:** 50966–50972.
4. MALASPINA, A. & J. de Belleroche. 2004. Spinal cord molecular profiling provides a better understanding of amyotrophic lateral sclerosis pathogenesis. Brain Res. Brain Res. Rev. **45:** 213–229.
5. YOSHIHARA, T., S. ISHIGAKI, M. YAMAMOTO, *et al.* 2002. Differential expression of inflammation- and apoptosis-related genes in spinal cords of a mutant SOD1 transgenic mouse model of familial amyotrophic lateral sclerosis. J. Neurochem. **80:** 158–167.
6. KATO, K. 1995. Description of the entire mRNA population by a 3′ end cDNA fragment generated by class IIS restriction enzymes. Nucleic Acids Res. **23:** 3685–3690.

7. NIWA, J., S. ISHIGAKI, M. DOYU, *et al.* 2001. A novel centrosomal ring-finger protein, dorfin, mediates ubiquitin ligase activity. Biochem. Biophys. Res. Commun. **281:** 706–713.
8. BOHM, C., D. NEWRZELLA & O. SORGENFREI. 2005. Laser microdissection in CNS research. Drug Discov. Today **10:** 1167–1174.
9. JIANG, Y.M., M. YAMAMOTO, Y. KOBAYASHI, *et al.* 2005. Gene expression profile of spinal motor neurons in sporadic amyotrophic lateral sclerosis. Ann. Neurol. **57:** 236–251.
10. HALL, E.D., J.A. OOSTVEEN & M.E. GURNEY. 1998. Relationship of microglial and astrocytic activation to disease onset and progression in a transgenic model of familial ALS. Glia **23:** 249–256.
11. GRAY, F., H. ADLE-BIASSETTE, F. BRION, *et al.* 2000. Neuronal apoptosis in human immunodeficiency virus infection. J. Neurovirol. **6:** S38–S43.
12. MINGHETTI, L. & G. LEVI. 1998. Microglia as effector cells in brain damage and repair: focus on prostanoids and nitric oxide. Prog. Neurobiol. **54:** 99–125.
13. ANDO, Y., Y. LIANG, S. ISHIGAKI, *et al.* 2003. Caspase-1 and -3 mRNAs are differentially upregulated in motor neurons and glial cells in mutant SOD1 transgenic mouse spinal cord: a study using laser microdissection and real-time RT-PCR. Neurochem. Res. **28:** 839–846.
14. ISHIGAKI, S., Y. LIANG, M. YAMAMOTO, *et al.* 2002. X-linked inhibitor of apoptosis protein is involved in mutant SOD1-mediated neuronal degeneration. J. Neurochem. **82:** 576–584.
15. NIWA, J., S. ISHIGAKI, N. HISHIKAWA, *et al.* 2002. Dorfin ubiquitylates mutant SOD1 and prevents mutant SOD1-mediated neurotoxicity. J. Biol. Chem. **277:** 36793–36798.
16. ISHIGAKI, S., N. HISHIKAWA, J. Niwa, *et al.* 2004. Physical and functional interaction between Dorfin and Valosin-containing protein that are colocalized in ubiquitylated inclusions in neurodegenerative disorders. J. Biol. Chem. **279:** 51376–51385.
17. TAKEUCHI, H., J. NIWA, N. Hishikawa, *et al.* 2004. Dorfin prevents cell death by reducing mitochondrial localizing mutant superoxide dismutase 1 in a neuronal cell model of familial amyotrophic lateral sclerosis. J. Neurochem. **89:** 64–72.
18. ISHIGAKI, S., J. NIWA, T. YOSHIHARA, *et al.* 2000. Two novel genes, human neugrin and mouse m-neugrin, are upregulated with neuronal differentiation in neuroblastoma cells. Biochem. Biophys. Res. Commun. **279:** 526–533.
19. LUO, L., R.C. SALUNGA, H. GUO, *et al.* 1999. Gene expression profiles of laser-captured adjacent neuronal subtypes. Nat. Med. **5:** 117–122.
20. Van GELDER, R.N., M.E. VON ZASTROW, A. YOOL, *et al.* 1990. Amplified RNA synthesized from limited quantities of heterogeneous cDNA. Proc. Natl. Acad. Sci. USA **87:** 1663–1667.
21. PULS, I., C. JONNAKUTY, B.H. LAMONTE BH, *et al.* 2003. Mutant dynactin in motor neuron disease. Nat. Genet. **33:** 455–456.
22. PULS, I., S.J. OH, C.J. SUMNER, *et al.* 2005. Distal spinal and bulbar muscular atrophy caused by dynactin mutation. Ann. Neurol. **57:** 687–694.
23. Levy, J.R., C.J. SUMNER, J.P. Caviston, *et al.* 2006. A motor neuron disease-associated mutation in p150Glued perturbs dynactin function and induces protein aggregation. J. Cell. Biol. **172:** 733–745.

24. FARAH, C.A., M.D. NGUYEN, J.P. JULIEN, *et al.* 2003. Altered levels and distribution of microtubule-associated proteins before disease onset in a mouse model of amyotrophic lateral sclerosis. J. Neurochem. **84:** 77–86.
25. WAZA, M., H. ADACHI, M. KATSUNO, *et al.* 2005. 17-AAG, an Hsp90 inhibitor, ameliorates polyglutamine-mediated motor neuron degeneration. Nat. Med. **11:** 1088–1095.
26. THE 21ST CENTURY COE PROGRAM: Integrated Molecular Medicine for Neuronal and Neoplastic Disorders. http://www.nagoya-u.ac.jp/coemed/.

Neurobiology of Disease

Reversible Disruption of Dynactin 1-Mediated Retrograde Axonal Transport in Polyglutamine-Induced Motor Neuron Degeneration

Masahisa Katsuno, Hiroaki Adachi, Makoto Minamiyama, Masahiro Waza, Keisuke Tokui, Haruhiko Banno, Keisuke Suzuki, Yu Onoda, Fumiaki Tanaka, Manabu Doyu, and Gen Sobue

Department of Neurology, Nagoya University Graduate School of Medicine, Showa-ku, Nagoya 466-8550, Japan

Spinal and bulbar muscular atrophy (SBMA) is a hereditary neurodegenerative disease caused by an expansion of a trinucleotide CAG repeat encoding the polyglutamine tract in the *androgen receptor* (*AR*) gene. To elucidate the pathogenesis of polyglutamine-mediated motor neuron dysfunction, we investigated histopathological and biological alterations in a transgenic mouse model of SBMA carrying human pathogenic AR. In affected mice, neurofilaments and synaptophysin accumulated at the distal motor axon. A similar intramuscular accumulation of neurofilament was detected in the skeletal muscle of SBMA patients. Fluoro-gold labeling and sciatic nerve ligation demonstrated an impaired retrograde axonal transport in the transgenic mice. The mRNA level of dynactin 1, an axon motor for retrograde transport, was significantly reduced in the SBMA mice resulting from pathogenic AR-induced transcriptional dysregulation. These pathological events were observed before the onset of neurological symptoms, but were reversed by castration, which prevents nuclear accumulation of pathogenic AR. Overexpression of dynactin 1 mitigated neuronal toxicity of the pathogenic AR in a cell culture model of SBMA. These observations indicate that polyglutamine-dependent transcriptional dysregulation of dynactin 1 plays a crucial role in the reversible neuronal dysfunction in the early stage of SBMA.

Key words: polyglutamine; spinal and bulbar muscular atrophy; androgen; neurofilament; axonal transport; retrograde; dynactin

Introduction

Spinal and bulbar muscular atrophy (SBMA), or Kennedy's disease, is a hereditary neurodegenerative disease resulting from a loss of bulbar and spinal motor neurons (Kennedy et al., 1968; Sobue et al., 1989). Patients present with muscle atrophy and weakness of proximal limbs associated with bulbar palsy, tongue atrophy and contraction fasciculation (Katsuno et al., 2006). The disease affects exclusively adult males, whereas females carrying the mutant *androgen receptor* (*AR*) are seldom symptomatic (Schmidt et al., 2002). The molecular basis of SBMA is an expansion of a trinucleotide CAG repeat, which encodes the polyglutamine tract in the first exon of the *AR* gene (La Spada et al., 1991). This type of mutation has also been found to cause a variety of neurodegenerative disorders, termed polyglutamine diseases, such as Huntington's disease (HD), several forms of spinocerebellar ataxia, and dentatorubral pallidoluysian atrophy (Gatchel and Zoghbi, 2005). Although expression of the causative gene in each of these diseases is ubiquitous, selective neuronal cell death is observed in disease-specific areas of the CNS, suggesting a common molecular basis for these polyglutamine diseases.

Nuclear accumulation of pathogenic protein containing elongated polyglutamine is a crucial step in the pathophysiology of these diseases, providing an important therapeutic target (Adachi et al., 2005; Banno et al., 2006). The aberrant polyglutamine protein has a propensity to form aggregates in the nucleus and inhibits the function of transcriptional factors and coactivators, resulting in transcriptional perturbation (Cha, 2000; Gatchel and Zoghbi, 2005). In support of this hypothesis, altered expression of a variety of genes has been demonstrated in transgenic mouse models of polyglutamine diseases (Sugars and Rubinsztein, 2003). Although polyglutamine-induced transcriptional dysregulation is likely to be central to the pathogenesis of polyglutamine diseases, it has yet to be elucidated which genes are responsible for the selective neurodegeneration (Gatchel and Zoghbi, 2005).

No treatments have been established for polyglutamine diseases, but the androgen blockade therapy, surgical or medical castration, has shown striking therapeutic effects in the SBMA transgenic mouse model (Katsuno et al., 2002, 2003; Chevalier-Larsen et al., 2004). Androgen deprivation strongly inhibits the ligand-dependent nuclear accumulation of pathogenic AR protein, resulting in a striking improvement in neurological and histopathological findings of male mice.

In the present study, we investigated the molecular pathophysiology of motor neuron dysfunction in a transgenic mouse

Received July 18, 2006; revised Sept. 21, 2006; accepted Oct. 6, 2006.

This work was supported by a Center of Excellence grant from the Ministry of Education, Culture, Sports, Science and Technology, Japan, and by grants from the Ministry of Health, Labor and Welfare, Japan. We have no financial conflict of interest that might be construed to influence the results or interpretation of this manuscript. We thank Jun-ichi Miyazaki for kindly providing the pCAGGS vector.

Correspondence should be addressed to Dr. Gen Sobue, Department of Neurology, Nagoya University Graduate School of Medicine, 65 Tsurumai-cho, Showa-ku, Nagoya 466-8550, Japan. E-mail: sobueg@med.nagoya-u.ac.jp.

DOI:10.1523/JNEUROSCI.3032-06.2006

 0270-6474/06/2612106-12$15.00/0

model of SBMA. Polyglutamine-induced transcriptional dysregulation of the dynactin p150 subunit (dynactin 1), an axonal motor-associated protein, resulted in perturbation of retrograde axonal transport in spinal motor neurons in the early stage of the disease. These processes were reversed by castration, which inhibits nuclear accumulation of pathogenic AR. A defect in axonal trafficking of neurofilaments and synaptic vesicles, the potential molecular basis for the reversible pathogenesis, appears to contribute to the initiation of symptoms, and may account for the selective degeneration of motor neurons in SBMA.

Materials and Methods

Generation and maintenance of transgenic mouse. AR-24Q and AR-97Q mice were generated as described previously (Katsuno et al., 2002). Briefly, the full-length human *AR* fragment harboring 24 or 97 CAGs was subcloned into the *Hind*III site of the pCAGGS vector (Niwa et al., 1991) and microinjected into BDF1-fertilized eggs. Five founders with AR-97Q were obtained. These mouse lines were maintained by backcrossing them to C57BL/6J mice. All symptomatic lines (2–6, 4–6, and 7–8) were examined in the present study. All animal experiments were approved by the Animal Care Committee of the Nagoya University Graduate School of Medicine. Mice were given sterile water *ad libitum*. In the experiments where it was called for, sodium butyrate [a histone deacetylase (HDAC) inhibitor] was administered at a concentration of 4 g/L in distilled water from 5 weeks of age until the end of the analysis, as described previously (Minamiyama et al., 2004).

Neurological testing and castration after onset. Mice were subjected to the Rotarod task (Economex Rotarod; Colombus Instruments, Columbus, OH), and cage activity was measured (AB system; Neuroscience, Tokyo, Japan) as described previously (Katsuno et al., 2002). Gait stride was measured in 50 cm of footsteps, and the maximum value was recorded for each mouse. The onset of motor impairment was determined using weekly rotarod task analyses. Male AR-97Q mice were castrated or sham-operated via the abdominal route under ketamine–xylazine anesthesia (50 mg/kg ketamine and 10 mg/kg xylazine, i.p.) within 1 week after the onset of rotarod impairment.

Immunohistochemistry and immunofluorescent analysis. Ten-micrometer-thick sections were prepared from paraffin-embedded tissues, and immunohistochemistry was performed as described previously (Katsuno et al., 2002). Formalin-fixed tail samples were washed with 70% ethanol and decalcified with 7% formic acid–70% ethanol for 7 d before embedding in paraffin. Sections to be immunostained for dynactin 1, dynein intermediate chain, dynein heavy chain, and dynamitin were first microwaved for 20 min in 50 mM citrate buffer, pH 6.0. Sections to be immunostained for polyglutamine (1C2 antibody) were treated with formic acid for 5 min at room temperature. The following primary antibodies were used: anti-dynactin 1 (p150^{glued}, 1:250; BD Transduction, San Diego, CA), anti-dynein intermediate chain (1:500; Millipore, Temecula, CA), anti-dynein heavy chain (1:100; Sigma-Aldrich, St. Louis, MO), anti-dynamitin (1:1000; BD Transduction), anti-polyglutamine, 1C2 (1:10,000; Millipore), antiphosphorylated high molecular weight neurofilament (NF-H) (SMI31, 1:1000; Sternberger Monoclonals, Lutherville, MD), anti-nonphosphorylated NF-H (SMI32, 1:5000; Sternberger Monoclonals), and anti-synaptophysin (1:10,000; Dako, Glostrup, Denmark).

For immunofluorescent analysis of skeletal muscle, mice were deeply anesthetized with ketamine–xylazine and perfused with PBS followed by 4% paraformaldehyde fixative in phosphate buffer, pH 7.4. Gastrocnemius muscles were dissected free, frozen quickly by immersion in cooled acetone and powdered CO_2. Longitudinal, 30 μm, cryostat sections were placed on a silane-coated slide in a drop of 3% disodium EDTA, air dried at room temperature, and fixed in methanol/acetone (50:50 v/v). After blocking with PBS containing 5% goat serum and 1% BSA for 30 min at room temperature, sections were incubated with 5 μg/ml Oregon green-conjugated α-bungarotoxin (Invitrogen, Eugene, OR) for 60 min at room temperature. Sections were incubated with antiphosphorylated NF-H (SMI31, 1:5000; Sternberger Monoclonals), anti-synaptophysin (1:50,000; Dako), or anti-Rab3A (1:5000; BD Transduction) antibodies at 4°C overnight, and then with Alexa-546-conjugated goat anti-mouse IgG (1:1000; Invitrogen). Sections were examined with an IX71 inverted microscope (Olympus, Tokyo, Japan). For double staining of the skeletal muscle, paraffin-embedded sections were treated with TNB blocking buffer (PerkinElmer, Boston, MA) and incubated with anti-AR antibody (N-20, 1:500; Santa Cruz Biotechnology, Santa Cruz, CA) together with antiphospho-NF-H.

For immunostaining of human tissues, autopsy specimens of lumbar spinal cord and intercostal muscle obtained from a genetically diagnosed SBMA patient (78-year-old male) and those from a neurologically normal patient (75 years old) were used. The collection of tissues and their use for this study were approved by the Ethics Committee of Nagoya University Graduate School of Medicine. Spinal cord sections at 10 μm were incubated with anti-dynactin 1 antibody (p150^{glued}, 1:250; BD Transduction). Thirty-micrometer-thick cryostat sections of intercostal muscle were incubated with 150 μg/ml Alexa-488-conjugated α-bungarotoxin (Invitrogen) and then with antiphosphorylated NF-H (SMI31, 1:200; Sternberger Monoclonals).

Retrograde Fluoro-gold neurotracer labeling. For labeling neurons with intramuscular injection of tracer, mice were anesthetized with ketamine–xylazine, and a small incision was made in the skin of the left calf to expose the gastrocnemius muscle. A total volume of 4.5 μl of 2.5% Fluoro-gold solution (Biotium, Hayward, CA) in PBS was injected in three different parts of the muscle (proximal, middle, and distal) using a 10 μl Hamilton syringe. For labeling by the nerve stump method, the sciatic nerve was exposed and transected at mid-thigh level. A small polyethylene tube containing 2.5% Fluoro-gold solution was applied to the proximal stump of the cut sciatic nerve, and sealed with Vaseline to prevent leakage. Mice were anesthetized 44 h after Fluoro-gold administration with ketamine–xylazine and perfused with PBS followed by 4% paraformaldehyde in phosphate buffer, pH 7.4. Spinal cords were removed and postfixed with 4% paraformaldehyde in phosphate buffer for 2 h, floated in 10 and 15% sucrose for 4 h each and in 20% sucrose overnight. The samples were sectioned longitudinally on a cryostat at 30 μm and mounted on silane-coated slides. The number of Fluoro-gold labeled motor neurons was counted in serial spinal cord sections with an IX71 inverted microscope (Olympus) using a wide-band UV filter. Some specimens were immunostained for dynactin immediately after the number of Fluoro-gold-labeled motor neurons was counted.

Western blot analysis. SH-SY5Y cells were lysed in CellLytic lysis buffer (Sigma-Aldrich) containing a protease inhibitor mixture (Roche, Mannheim, Germany) 2 d after transfection. Mice were killed under ketamine–xylazine anesthesia. Their tissues were snap-frozen with powdered CO_2 in acetone and homogenized in 50 mM Tris, pH 8.0, 150 mM NaCl, 1% NP-40, 0.5% deoxycholate, 0.1% SDS, and 1 mM 2-mercaptoethanol containing 1 mM PMSF and 6 μg/ml aprotinine and then centrifuged at 2500 × *g* for 15 min at 4°C. The supernatant fractions were separated on 5–20% SDS-PAGE gels (10 μg protein for the nerve roots or 40 μg for the spinal cord, per lane) and then transferred to Hybond-P membranes (Amersham Pharmacia Biotech, Buckinghamshire, UK), using 25 mM Tris, 192 mM glycine, 0.1% SDS, and 10% methanol as transfer buffer. Immunoblotting was performed using the following primary antibodies: anti-dynactin 1 (p150^{glued}, 1:250; BD Transduction), anti-dynein intermediate chain (1:1000; Millipore), anti-dynein heavy chain (1:200; Sigma-Aldrich), anti-dynamitin (1:250; BD Transduction), anti-α-tubulin (1:5000; Sigma-Aldrich), antiphosphorylated NF-H (SMI31, 1:100,000; Sternberger Monoclonals), and anti-nonphosphorylated NF-H (SMI32, 1:1000; Sternberger Monoclonals). The immunoblots were digitalized (LAS-3000 imaging system; Fujifilm, Tokyo, Japan), signal intensities of three independent blots were quantified with Image Gauge software version 4.22 (Fujifilm), and the means ± SD were expressed in arbitrary units.

Ligation of mouse sciatic nerve. Under anesthesia with ketamine–xylazine, the skin of the right lower limb was incised. The right sciatic nerve was exposed and ligated at mid-thigh level using surgical thread. For immunofluorescent analysis, operated mice were decapitated under deep anesthesia with ketamine–xylazine 8 h after ligation and perfused with 4% paraformaldehyde fixative in phosphate buffer, pH 7.4. The right sciatic nerve segment, including at least 5 mm both proximal and distal to

the ligated site, was removed. The nonligated, left sciatic nerve was also taken out in the same manner as the right nerve. The removed nerves were placed into fixative for 4 h, transferred consecutively to 10, 15, and 20% sucrose in 0.01 M PBS, pH 7.4, for 4 h each at 4°C, mounted in Tissue-Tek OCT compound (Sakura, Tokyo, Japan), and frozen with powdered CO_2 in acetone. Ten-micrometer-thick cryostat sections were prepared from the frozen tissues, blocked with normal goat serum (1:20), incubated with anti-synaptophysin (1:50,000; Dako) at 4°C overnight, and then with Alexa-546-conjugated goat anti-mouse IgG (1:1000; Invitrogen). Immunofluorescent images were recorded with an IX71 inverted microscope (Olympus), and the signal intensities were quantified using Image Gauge software, version 4.22 (Fujifilm) and expressed in arbitrary units.

For immunoblotting of axonal proteins, the sciatic nerve segments 1 mm both proximal and distal to the ligated site were removed without paraformaldehyde fixation, and frozen in with powdered CO_2 in acetone. Protein extraction and Western blotting were performed as described above.

In situ *hybridization.* Formalin-fixed, paraffin-embedded 6-μm-thick sections of the spinal cord were deparaffinized, treated with proteinase K, and processed for *in situ* hybridization using an ISHR kit (Nippon Gene, Tokyo, Japan) according to the manufacturer's instructions. Dynactin 1 cDNA was obtained from spinal cords of wild-type mice. The primers, 5′-AGATGGTGGAGATGCTGACC-3′ and 5′-GAGCCTTGGTCTCAGCAAAC-3′, were phosphorylated with T4polynucleotide kinase (Stratagene Cloning Systems, La Jolla, CA). The cDNA was inserted into the pSPT 19 vector (Roche). Dioxigenin-labeled cRNA antisense and sense probes, 380 bp long, were generated from this plasmid using T7 and SP6 polymerase (Roche), respectively. Spinal cord sections were hybridized for 16 h at 42°C washed in formamide–4× SSC (50:50 v/v) at the same temperature, treated with RNase A at 37°C, and washed again in 0.1× SSC at 42°C. The signals were detected immunologically with alkaline phosphatase-conjugated anti-dioxigenin antibody and incubated with NBT/BCIP (Roche) for 16 h at 42°C. Slices were counterstained with methyl green. To quantify the intensity of the signals in the cell bodies of spinal motor neurons, three nonconsecutive sections from a wild-type littermate and those of a transgenic mouse from lines 7–8 or 4–6 were analyzed using the NIH Image program (version 1.62). Sections adjacent to those used for *in situ* hybridization were processed for immunohistochemistry using anti-polyglutamine antibody as described above.

Quantitative real-time PCR. Dynactin 1 mRNA levels were determined by real-time PCR as described before (Ishigaki et al., 2002; Ando et al., 2003). Briefly, total RNA (5 μg each) from AR-97Q and wild-type spinal cord were reverse transcribed into first-strand cDNA using SuperScript II reverse transcriptase (Invitrogen). Real-time PCR was performed in a total volume of 50 μl, containing 25 μl of 2× QuantiTect SYBR Green PCR Master Mix and 0.4 μM of each primer (Qiagen, Valencia, CA), and the product was detected by the iCycler system (Bio-Rad Laboratories, Hercules, CA). The reaction conditions were 95°C for 15 min and then 45 cycles of 15 s at 95°C followed by 60 s at 55°C. For an internal standard control, the expression level of glyceraldehyde-3-phosphate dehydrogenase (GAPDH) was simultaneously quantified. The following primers used were 5′-CTCAGAGGAGCCCAGATGA-3′ and 5′-GCTGGTCTTGCGGTACAGT-3′ for dynactin 1, 5′-GAGAGCATGGAGCTGGTGTA-3′ and 5′-CCAACCACGAAGTTGTTGAC-3′ for dynein intermediate chain, 5′-TACCAGGTGGGAGTGCATTA-3′ and 5′-CAGTCACTATGCCCATGACC-3′ for dynein heavy chain, 5′-ACAAGCGTGGAACACATCAT-3′ and 5′-TCTTTCCAATGCGATCTGAG-3′ for dynamitin, and 5′-CCTGGAGAAACCTGCCAAGTAT-3′ and 5′-TGAAGTCGCAGGAGACAACCT-3′ for GAPDH. The threshold cycle of each gene was determined as the number of PCR cycles at which the increase in reporter fluorescence was 10 times the baseline signal. The weight of the gene contained in each sample was equal to the log of the starting quantity and the standardized expression level in each mouse was equal to the weight ratio of each gene to that of GAPDH.

For the real-time PCR with mRNA extracted from SH-SY5Y cells, the following primers were used: 5′-CTTGGAAGCGATGAATGAGA-3′ and 5′-TAGTCTGCAACGTCTCCTG-3′ for dynactin 1, and 5′-AGCCTCAAGATCATCAGCAAT-3′ and 5′-GGACTGTGGTCATGAGTCCTT-3′ for GAPDH.

Plasmid vectors and cell culture. Human AR cDNAs containing 24 or 97 CAG repeats were subcloned into pcDNA3.1 (Invitrogen) as described previously (Kobayashi et al., 2000). Human dynactin 1 cDNA was also subcloned into pcDNA3.1 (Invitrogen). The human neuroblastoma cells (SH-SY5Y, #CRL-2266; American Type Culture Collection, Manassas, VA) were plated in 6-well dishes in 2 ml of DMEM/F12 containing 10% fetal bovine serum with penicillin and streptomycin, and each dish was transfected with 2 μg of the vector containing AR24, AR97, or mock and with 2 μg of the vector containing dynactin 1 or mock using Opti-MEM (Invitrogen) and Lipofectamine 2000 (Invitrogen) and then differentiated in differentiation medium (DMEM/F12 supplemented with 5% fetal calf serum and 10 μM retinoic acid) for 2 d. Two days after transfection, cells were stained with propidium iodide (Invitrogen, Eugene, OR) and mounted in Gelvatol. Quantitative analyses were made from triplicate determinations. Duplicate slides were graded blindly in two independent trials as described previously (Katsuno et al., 2005).

Statistical analyses. We analyzed data using the Kaplan-Meier and log-rank test for survival rate, ANOVA with *post hoc* test (Dunnett) for multiple comparisons, and an unpaired *t test* from Statview software version 5 (Hulinks, Tokyo, Japan).

Results

Accumulation of axonal proteins in distal motor axons of SBMA mouse

To clarify the molecular basis of neuronal dysfunction in SBMA, we analyzed histopathological alterations in the spinal cords of transgenic mice carrying full-length human *AR* with 97 CAGs (AR-97Q mice) (Katsuno et al., 2002, 2003). We first focused on the expression and phosphorylation level of NF-H because affected mice demonstrate axonal atrophy in the ventral nerve root (Katsuno et al., 2002). Although it has been widely accepted that NF-H phosphorylation is a crucial factor determining axon caliber, neither the amounts nor the phosphorylation levels of NF-H in spinal cord or ventral root were decreased in male AR-97Q mice compared with wild-type littermates (supplemental Fig. 1*A–C*, available at www.jneurosci.org as supplemental material). The distribution of NF-H in the anterior horn of AR-97Q mice was also indistinguishable from that of wild-type or AR-24Q mice bearing human AR with a normal polyglutamine length (Fig. 1*A*). However, AR-97Q mice demonstrated a striking accumulation of both phosphorylated and nonphosphorylated NF-H in skeletal muscle, a phenomenon not observed in AR-24Q or wild-types (Fig. 1*A*). Although motor neurons originating in the anterior horn are always affected in SBMA, because the primary motor neurons projecting their axons to the anterior horn are not affected, no accumulation is seen in this region. The damage to motor neurons originating within the anterior horn results in accumulation of NFs in the skeletal muscle, instead of the spinal cord. A similar accumulation of the middle molecular weight NF was also observed (data not shown). To clarify whether this phenomenon is specific to neurofilaments, we performed immunohistochemistry on both spinal cord and muscle with an antibody against synaptophysin, a transmembrane glycoprotein of synaptic vesicles that is also retrogradely transported in axons (Li et al., 1995). In AR-97Q mice, synaptophysin accumulated among the muscle fibers in a pattern similar to that of NF-H, whereas no such accumulation was observed in unaffected mice (Fig. 1*B*).

We then investigated the time course of abnormally accumulated NF in skeletal muscle. Because the onset of motor dysfunction occurs at 9–10 weeks in AR-97Q mice, NF pathology before and after the onset was examined. Anti-NF immunostaining demonstrated that intramuscular NF accumulation was detectable as early as 7 weeks before the onset of muscle weakness in this